Development and optimization of Laser Shock Repeated Dense Peening (LSRDP) using most advanced laser architectures

Alexandre Rondepierre, Olivier Casagrande, Yann Rouchausse, Olivier Castelnau, Laurent Berthe

HAL Id: hal-03709627

https://hal.science/hal-03709627

Development and optimization of Laser Shock Repeated Dense Peening (LSRDP) using most advanced laser architectures

ALEXANDRE RONDEPIERRE,[1,2,*] **OLIVIER CASAGRANDE,**[2] **YANN ROUCHAUSSE,**[1] **OLIVIER CASTELNAU,**[1] **AND LAURENT BERTHE**[1]

[1] *Laboratoire Procédés et Ingénierie en Mécanique et Matériaux (PIMM), UMR8006 ENSAM, CNRS, CNAM, 151 bd de l'Hôpital, 75013 Paris, France*
[2] *THALES LAS France, 78990 Elancourt, France*
*alexandre.rondepierre@fr.thalesgroup.com

Abstract: The laser shock peening process (LSP), used to reinforce metals, currently has two major configurations with limitations. (1) Laser irradiation with large spot sizes, but with the need to use a thermal protective coating to avoid detrimental thermal damage (which increases the overall cost of the process) or (2) laser irradiation without thermal coating but with very small spot sizes and high overlap ratios, thus increasing the amount of time required to treat a given surface. In this study, we develop a new faster configuration for the LSP process, which can be applied without a thermal coating, but is still effective regarding surface treatment time. A new laser system has been developed for this faster configuration and has been used to perform the LSP treatment of aluminum alloys at a high-repetition rate. This new DPSS Q-switched Nd:YAG laser, delivers 1 J of energy with a pulse duration from 7 to 21 ns at a very high frequency of 200 Hz. We also studied the laser/matter interaction, according to the laser pulse duration, energy, and its wavelength. The water confinement (ejection and renewing) was monitored while an air-blowing system was implemented to manage water issues identified with this new configuration. Altogether, we demonstrated that such a configuration is fully operational.

1. Introduction

High-energy (1-10 J systems) nanosecond pulsed lasers have enabled the development of many material surface treatment processes, some considered to be promising for shaping a more sustainable and greener society. Among them, we can find laser-induced shock applications such as the LAser Shock Adhesion Test (LASAT [1,2]) used both to certify bonded composites structures, and then spread their applications, or to dismantle bonded parts without any chemical products, for better recycling. Another important industrial application is the Laser Shock Peening (LSP [3–5]) process which helps to enhance both the fatigue life and the mechanical resistance of treated metals.

As drawn in Fig. 1, the LSP process consists in focusing a high-power laser pulse (ns-range duration) on the top of the material to be processed. The laser intensity locally reaches values above the GW/cm^2, thus the material is vaporized, ionized and transformed into a high-pressure and high-temperature plasma. As a result of the plasma expansion, a strong shock wave propagates inside the material, and plasticizes it, hence creating compressive residual stresses that fight against fatigue issues [6].

LSP is applied under the water confinement regime, which enables a greater pressure and a longer duration of the plasma compared to a direct interaction without confinement, as the confinement will slow down the plasma expansion [7,8]. As a consequence, pressures above the GPa are reached, which exceeds the elastic limit of most often used materials and allows their reinforcement.
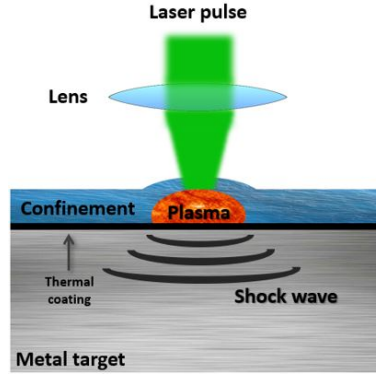
Fig. 1. Fundamental mechanism of LSP with thermal coating.

However, as the plasma reaches very high temperature ($\approx$10 000 K, [9]), a thermal protective coating has to be applied before the LSP treatment in order to protect the treated material from detrimental tensile residual stresses thermally induced. This reduces the potential of this process, compared to conventional Shot Peening [10], as the thermal coating increases its duration and its costs, especially in the aeronautical field where maintenance time can not be compressed.

Nevertheless, at the end of the 90's, Sano *et al.* developed the process without thermal coating (LSPwC, [11,12]) for underwater applications (such as reinforcement of steel welds in nuclear power reactor) as it was not possible to apply the thermal coating (because of gamma radiation this has to be a fully remote operation), and they demonstrated its effectiveness. As the laser beam was transported through an optical fiber, energies were limited (50 to 100 mJ) and small laser spots were used (0.4 to 0.8 mm) in order to keep the required laser intensity. Recent works have tried to explain the reasons for which LSPwC was working, and revealed the importance of using both a high overlap ratio and submillimeter laser spot sizes. Indeed, a mechanical analysis of residual stresses, spatially resolved through X-Ray diffraction, demonstrated that a high overlap ratio between shots is required, and a model was proposed [13]. Moreover, our previous study of the laser/matter interaction underlined the importance of using small laser spot sizes in order to shorten the plasma release duration so that thermal damages are drastically reduced [14].

These two main necessary conditions to make LSPwC effective imply some drawbacks regarding the average time required to treat a given surface. Indeed, this time (in m²/s) as function of the used laser radius R (m) and of the overlap ratio τ_r (expressed in %) is given by:

$$\eta_s = \frac{100\pi R^2 f}{\tau_r} \tag{1}$$

where f (Hz) is the laser frequency of treatment.

Hence, as LSPwC requires high values of τ_r and small values of R, it is necessary to increase the used frequency f of the laser to make it competitive compared to the classical LSP with thermal coating where small overlap ratios are used and large spot size ($\approx$ 5 mm) are employed.

Regarding the used laser systems with the thermal coating configuration, most of them were based on either Nd:Glass, Nd:YAG or Nd:YLF crystals and were operated in the fundamental frequency, in the infrared ($\approx$ 1 μm). From the 70's to the 90's, energies (5 to 30 J) and pulse durations (10 to 30 ns) have not changed, while the frequency has been increased from one shot every 10 minutes (2 mHz) to more than a thousand (5 Hz), making this process suitable for industrial applications [15]. Nowadays, compact DPSS (Diode-Pumped Solide State) systems are used, such as the Procudo from LSPT (10 J, 20 ns, 20 Hz).

For LSPwC, as the application was underwater, a green visible system (532 nm) was developed. This very-compact Nd:YAG system, carried through optical fiber, is based on the following parameters: 100 - 200 mJ, 5 - 10 ns and at 10 - 50 Hz.

Very recently, the Hilase Center in Czech Republic has been using and developing a Yb:YAG system (1 J, 10 ns, 10 Hz, [16]) and they demonstrated its suitability for LSP process. However, this cryogenically cooled system remains complex compared to a water cooled system.

Overall, it appears that there is a lack in high-frequency (> 100 Hz) and middle-energies (≈ 0.5 - 2 J) systems.

Altogether, our presented work aims at developing the process without any thermal coating, with high overlap ratios and submillimeter spot sizes, while keeping a fast time of treatment. A new DPSS laser system, delivering 1 J at 200 Hz and presented in the first part of this article, has been developed and is proposed to reach this objective. The tools and diagnoses used in our dedicated facility are also presented. On the other hand, we present new experimental results regarding the understanding of the process (laser/matter interaction and water confinement behavior at high repetition rate) in order to optimize it and to apply it to the reinforcement of aluminium alloys. This unpublished configuration at 200 Hz, with tough challenges but promising results, has finally been demonstrated to be viable and shall be known as Laser Shock Repeated Dense Peening (LSRDP).

2. Laser facility and experimental setup

2.1. Laser facility

2.1.1. THEIA laser

As our main objective was to perform LSP without coating (thus, as explained in the introduction, it requires to use small laser spots and high overlap ratios), while keeping an effective surface processing time, a high repetition rate laser (200 Hz) was developed and provided by Thales : the THEIA. This laser has suitable parameters for submillimeter LSP: the energy goes up to 1 J and the pulse duration ranges from 7 ns to 21 ns. Table 1 summarizes the possible parameters offered by the THEIA laser system.

Table 1. THEIA parameters.

Energy (mJ)	Pulse duration (FWHM, ns)	Wavelength (nm)	Repetition rate (Hz)
10 - 1050	6,9 - 21	1064	200

It consists in a MOPA (Master Oscillator Power Amplifier) architecture, with a Nd:YAG crystal rod being pumped by laser diodes and optically Q-switched with a pockels cell coupled to a quarter wavelength plate and a polarizer (Fig. 2). The created laser pulse exiting the oscillator is amplified through a main amplifier stage, also made from a Nd:YAG crystal rod pumped by diodes. Both crystal rods are water-cooled to manage the temperature.

Finally, the amplified beam goes towards an optical attenuator (made of a motorized half waveplate and a polarizer), so that the energy is tunable from 10 mJ to 1050 mJ.

The pulse duration of this system is tunable from 6.9 ns to 21 ns. This possibility is achieved by changing the optical gain available in the oscillator, so that the pulse is created more or less quickly. Indeed, reducing the pumping intensity of diodes will reduce the available gain and then it will increase the time needed for the laser pulse to be created and to extract the energy.

Furthermore, as the main amplifier is saturated, almost the same amount of energy is extracted by the seed pulse generated by the oscillator. As a consequence, this pulse-width tuning is done without sacrificing too much energy (1.05 J at 6.9 ns versus 0.73 J at 21 ns).
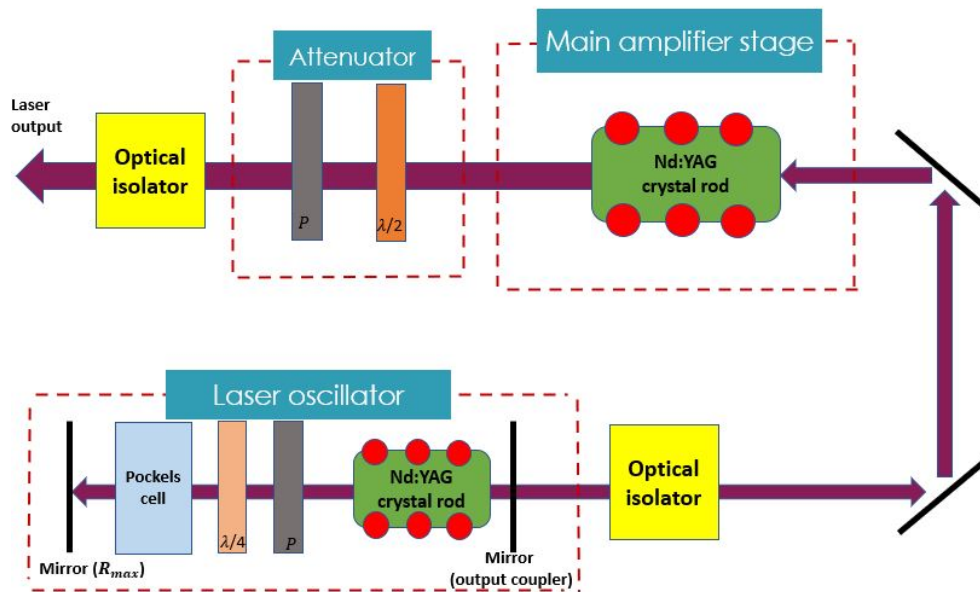
Fig. 2. Simplifed architecture of the THEIA laser.

2.1.2. Devices and equipments to perform laser shock treatments

Our experiments were performed at the Rogue Laser facility, in PIMM laboratory (Paris). It is an all-included platform for both characterization and treatment of laser shock peening, as represented in Fig. 3.

As the laser must be operated continuously at 200 Hz for thermal reasons, a galvanometer scanner mirror (from ScanLab) was employed to select single pulse for optical and mechanical analysis (detailed in part 2.2), but also to change LSP treatment frequencies from 1 Hz to 200 Hz. When no treatment or beam analysis is performed, the laser is sent in a water cooled dump.

Concerning LSP treatments, a robot arm (made by Kuka) was used to move the target in front of the fixed laser beam. Water confinement was supplied at various flow velocities (from 1 m/s to more than 6 m/s), as well as a blowing system was used (various air nozzles with an over-pressure from 0.1 MPa to 0.6 MPa) to protect optics and to clean the laser beam path.

Finally, as the laser beam obtained by the THEIA is top-hat in near field but gaussian in far field, the beam in far field (where it is focused into a small spot, required for the process) had to be spatially rendered top-hat, and smoothened, by using a DOE (diffractive optical element, made by Holoor). The beam size at the focal point (from 0.6 mm to 2 mm) was chosen by using various focal lengths (from +400 mm to + 1200 mm).

2.2. Optical and mechanical setup

2.2.1. Laser beam characterization

A pyroelectric detector (QE50LP-H-MB-QED from Gentec-EO) was used to measure the energy contained in one single laser pulse. A DET10A2 fast photodiode (from Thorlabs, rising time < 1 ns with 350 MHz of bandwidth) was used to acquire the laser pulse temporal duration (6.9 ns, 15 ns and 21 ns at FWHM, Fig. 4). Each measurements were averaged over 50 shots.

Furthermore, a CCD camera (acA2040-25gm from Basler) was employed to measure the spatial distribution of laser intensity obtained with the DOE. Images acquired for laser spot diameters of 0.72, 1.25 and 2 mm are plotted in Fig. 5.
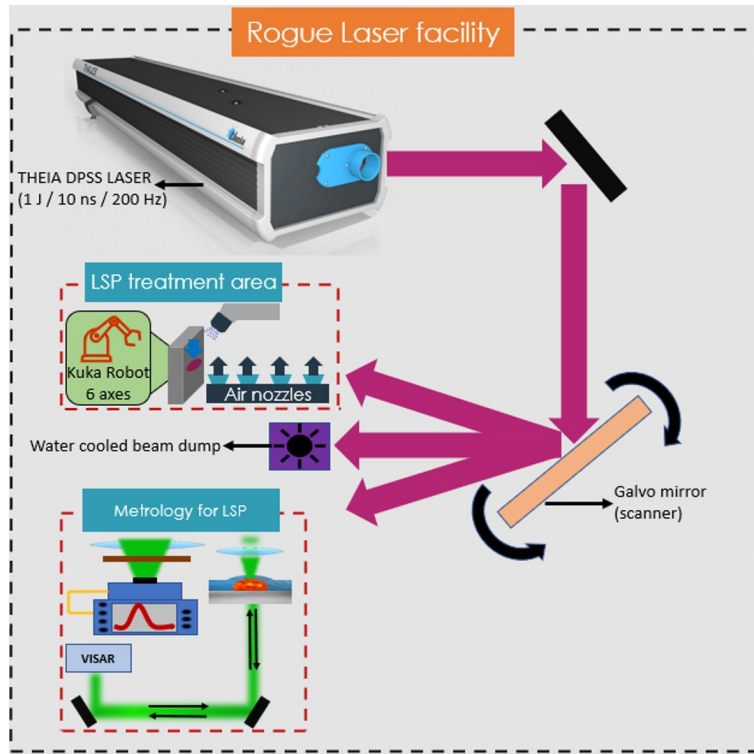
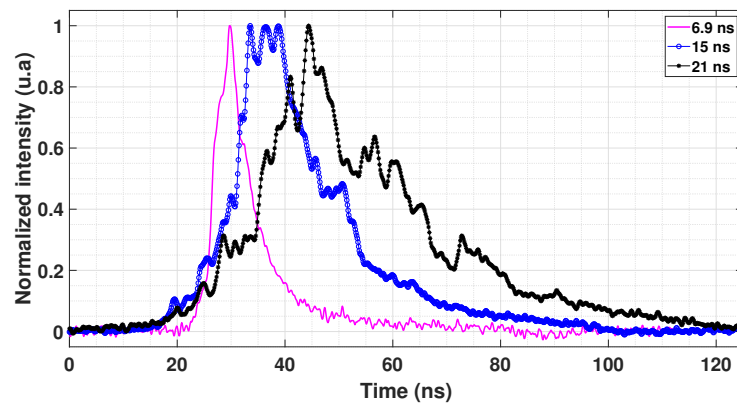**Fig. 3.** Schematic view of the Rogue Laser facility dedicated to LSP.

Fig. 4. Temporal pulse shapes used (6.9, 15, 21 ns).

2.2.2. Plasma pressure measurements with VISAR

Our previous works have already presented the way one can measure the laser-induced plasma pressure by using a VISAR [17] (simplified drawing in Fig. 6).

Based on a system developed by Barker [18], the main purpose is to measure the rear surface velocity of the metal target (this velocity being induced by the shock wave, itself generated by the high-pressure plasma) from the Doppler-Fizeau's shift of the laser probe wavelength.
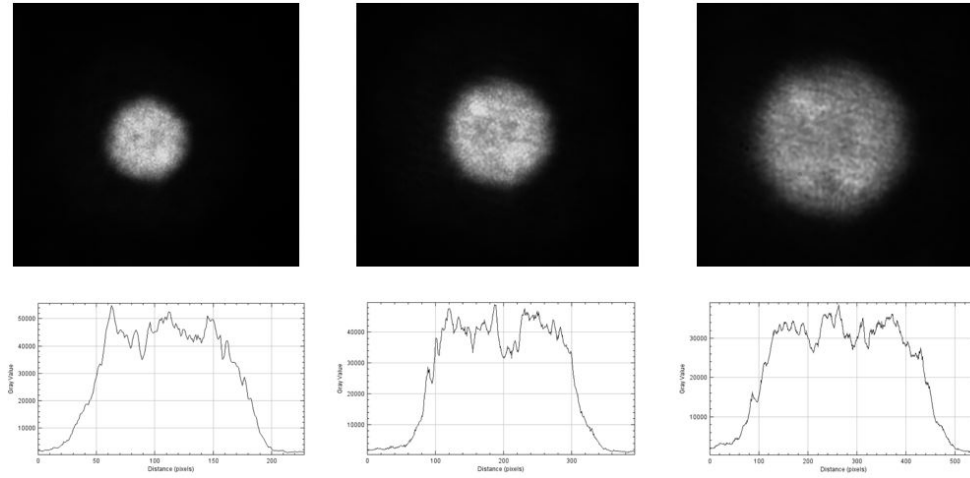
Fig. 5. Used laser spots with DOE (from left to right: 0.72 mm, 1.25 mm and 2 mm).
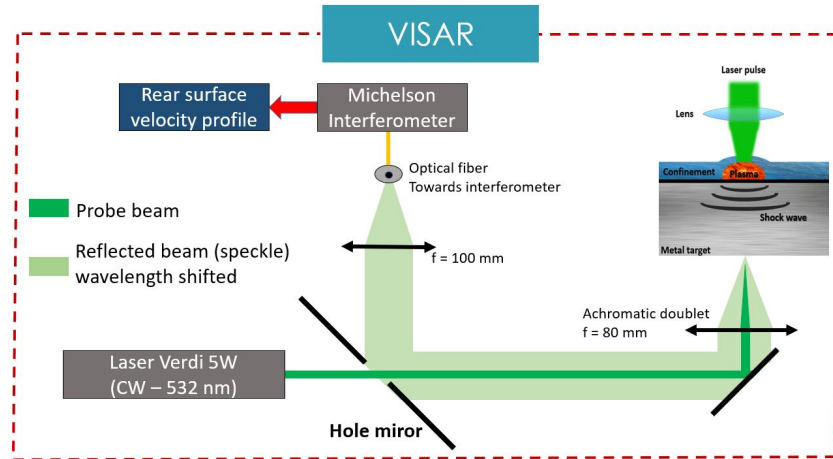

Fig. 6. Simplified principle of a VISAR

From this rear free surface velocity u_f, one can get the plasma pressure:

$$P_{\text{plasma}} = \frac{\rho(C_0 + S\frac{u_f}{2})u_f}{2} + \frac{2\sigma_{y_0}}{3} + \delta P \tag{2}$$

where ρ is the material density, C_0 the bulk sound velocity, S the Hugoniot constant, δP is the attenuation of the shock wave and $\frac{2\sigma_{y_0}}{3}$ the elastic contribution (σ_{y_0} being the elastic limit of the material).

2.2.3. High-speed camera observations

A high-speed camera (APX-RS, Photron) was used to observe both the renewing and the ejection of the water confinement after one laser shot. The pixel size of this camera is 17 μm, and various resolutions may be obtained depending on the used acquisition frequency (from 1024 x 1024 pixels to 128 x 16 pixels at 250 000 frames per second). The camera was externally triggered by the laser, and 1000 successive images could be recorded.

Cross-sectional observations were performed to get information on the way the water is ejected (velocities and angles, mainly), while a front view was employed to measure the time required for the flowing water to cover back the sample surface after one shot (renewing).

2.2.4. Residual stress measurements by X-Ray Diffraction

Residual stresses were measured by X-Ray $\sin^2(\Psi)$ diffraction method [19]. For that purpose, a 6-axis X-Raybot (made by MRXrays) was used. This system measures precisely the angle between the X-Ray source (k_α spectral line of Cr, $E = 5,41$ keV) and the diffracted beam, acquired by a semiconductor sensor.

In-depth measurements were achieved through successive electropolishing of the sample (saturated NaCl solution with a voltage of 30 V and a current of 3 A).

2.2.5. Sinking measurements

The method used to measure the specimen surface sinking after LSP is drawn in Fig. 7. Measurements were conducted with a Dektak 150 (Bruker) contact profilometer.
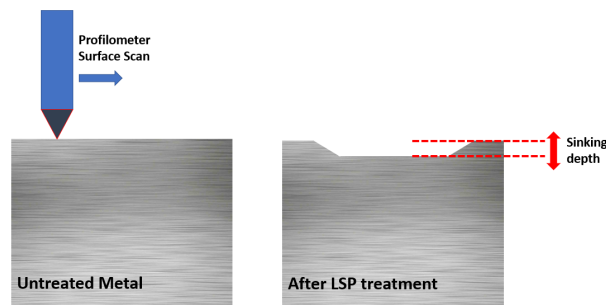

Fig. 7. Sinking measurement method.

Two mechanisms are responsible for the sample surface sinking: the pressure-induced plastic deformation [20] and the direct laser ablation of the surface [21]. Both phenomenon show a proportional dependency of the sinking with respect to the incident laser intensity reaching the target.

3. Study of Laser Mater Interaction through plasma pressure measurements: results

Pressure measurements were conducted as function of the laser spot size and as function of the laser pulse duration. Furthermore, a comparison was made between previous results at 532 nm and current one obtained with the THEIA at 1064 nm, as commonly used for the LSP process either in research works or industrial applications.

3.1. Plasma pressure as function of the laser spot size

We have plotted in Fig. 8 the results obtained for the plasma maximum reached pressure, as function of the laser intensity, for various laser spot sizes: 0.72 mm, 1.25 mm and 2 mm. This was obtained with a gaussian pulse duration (FWHM) of 6.9 ns.

These results show that the maximum pressure reached by the plasma is not depending on the used laser spot size, in agreement with our previous model that stated that only the release part of the plasma pressure would be affected by the laser spot size [14].
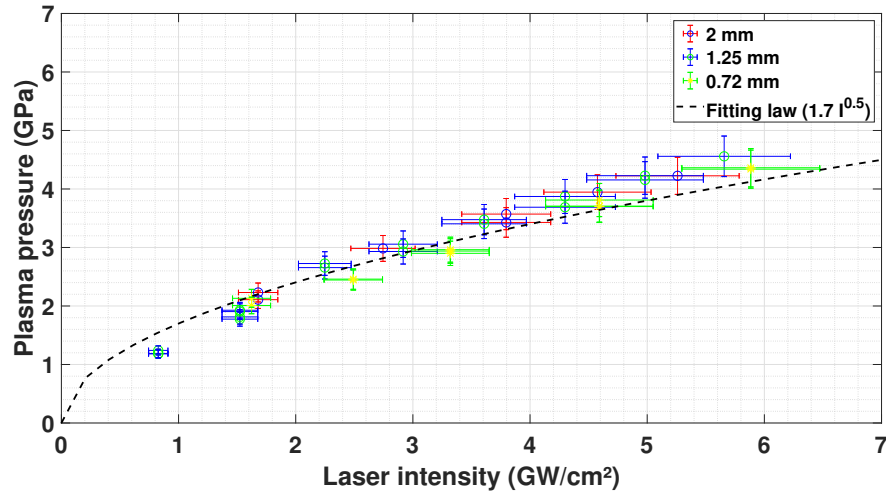
Fig. 8. Plasma pressure (GPa) as function of the laser intensity (GW/cm^2) for different spot sizes: 0.72 mm, 1.25 mm and 2 mm, with a pulse duration (FWHM) of 6.9 ns.

The analytical model from Fabbro [8] gives the following law for the maximum plasma pressure P_{max} (GPa):

$$P_{\text{max}} = 0.01 \sqrt{\frac{\alpha Z}{2\alpha + 3}} \sqrt{I_{\text{laser}}} \tag{3}$$

where I_{laser} is the laser intensity in GW/cm^2, Z is the harmonic mean of the shock impedances (in g/cm^2/s) of the considered metal and confinement, and α is the fraction of the total plasma internal energy used as thermal energy.

Thus, the following law has been proposed to fit our data:

$$P_{\text{max}} \text{ (GPa)} = 1.7\sqrt{I \text{ (GW/cm}^2\text{)}} \tag{4}$$

This corresponds to $\alpha = 0.3$.

3.2. *Plasma pressure as function of the laser pulse duration*

While using a constant laser spot size of 0.72 mm, the plasma pressure as function of the laser intensity was also measured for 3 different pulse durations: 6.9 ns, 15 ns and 21 ns (Fig. 9).

The presented results, as function of the pulse duration, show the dependency induced on the breakdown threshold intensity. This breakdown phenomenon was previously studied [22] and consists in the creation of a plasma at the surface of the water layer used as confinement. As a results, when this breakdown occurs, the plasma pressure does no longer increase with the laser intensity. From Fig. 9, we can observe that as higher the pulse duration is, and as lower the breakdown threshold is. Indeed, thresholds were identified to be at 7, 5 and 4 GW/cm^2 for pulse durations of respectively 6.9, 15 and 21 ns. Then, pressures of saturation were respectively measured at 4.5, 3.6 and 3.2 GPa.

Moreover, before the breakdown phenomenon that saturates the plasma pressure happens, there is no dependency of the maximum plasma pressure with the used laser pulse duration. The same law as Eq. (4) has been used to fit the data.

These results are in a very good agreement with previous works on breakdown in dielectric medium, where it was shown that the breakdown threshold intensity I_{bk} is expected to be depending on the laser pulse duration τ with the following relation: $I_{bk} \propto \tau^{-0.5}$ [23].
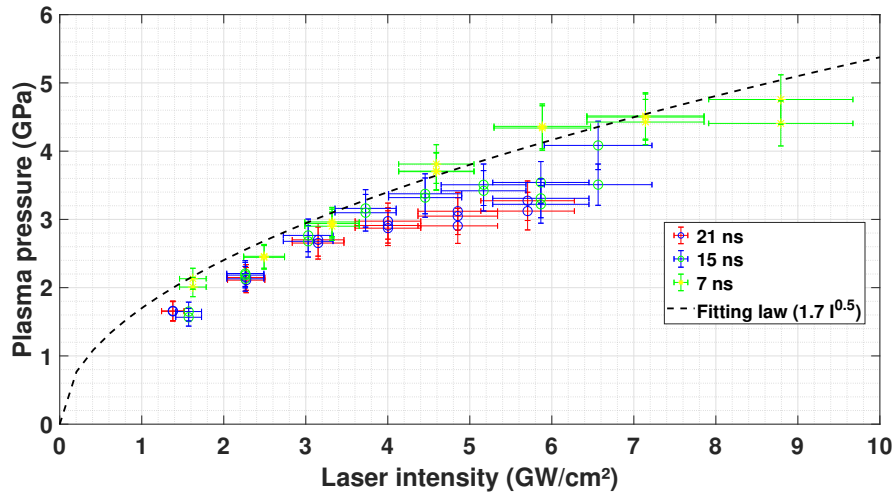
Fig. 9. Plasma pressure (GPa) as function of the laser intensity (GW/cm^2) for different pulse durations: 6.9 ns, 15 ns and 21 ns, with a laser spot size of 0.72 mm.

3.3. Plasma pressure as function of the laser wavelength

Pressure measurements and breakdown phenomenon for a gaussian laser pulse of 7 ns of duration (FWHM) were also characterized in a previous work [17], at 532 nm (second harmonic of Nd:YAG laser).

By comparing these two wavelengths (1064 nm and 532 nm, as plotted in Fig. 10), one can observe that the pressure (at constant intensity) is higher at 532 nm rather than at 1064 nm, because the α coefficient is also higher (0.6 versus 0.3): there is a better efficiency of interaction between the laser and the plasma at 532 nm, as mainly the critical density is higher so that the laser can penetrate deeper and bring more energy close to the sample surface. Altogether, as the absorption by Inverse Bremsstrahlung ([24]) is higher at shorter wavelength, this is why the pressure induced by the laser is higher at 532 nm than at 1064 nm (at constant laser intensity). This is consistent with previous results [25].

However, if one aims at comparing these two wavelengths as function of the initial laser energy, we can demonstrate that at least an efficiency of more than 60 % is required during SHG (Second Harmonic Generation) to make the choice of 532 nm better over 1064 nm. SHG is a nonlinear process during which the frequency of a laser is doubled. While the SHG efficiency is higher than 60 %, it is then possible to take advantage of this greater α coefficient, so that the generated pressure (at constant laser energy before SHG) is higher.

Altogether, as summarized in Table 2, it appears that the green wavelength of 532 nm is better for the process. Furthermore, this also allows to operate the process under water (as the beam is almost not absorbed at 532 nm while it is highly absorbed in the infrared) and to use the Water Tank configuration (several centimeters of water) for which the breakdown threshold intensity is doubled [17]. Nevertheless, in its most usual form, the LSP process is applied with a very thin layer of water confinement (as obtained in this work) with a thickness from 1 to 5 mm. In that case, the absorption in the infrared is considered to be negligible and does not affect the process (2 to 6 % of absorption).

However, for the presented work as various pulse durations were investigated (the SHG efficiency is worse with longer pulses) and as large spot sizes (2 mm) were used to be compared with small spot sizes, the infrared wavelength was kept. This enables to keep enough energy for
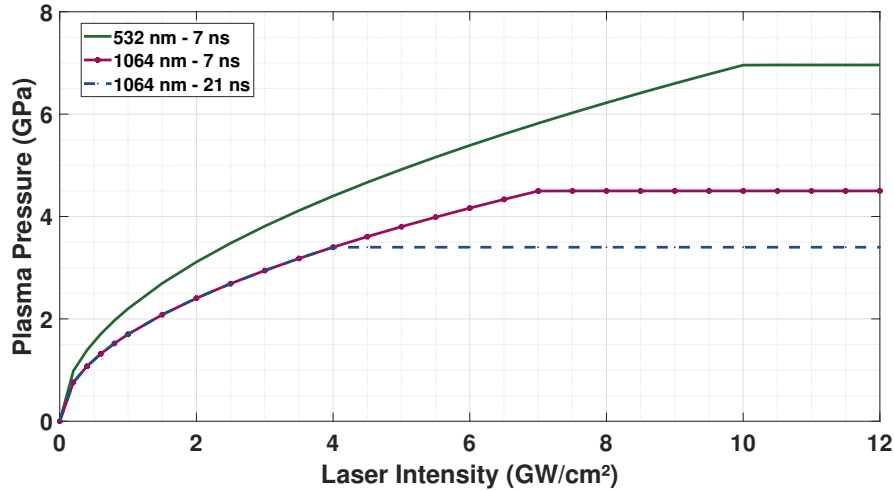
Fig. 10. Comparison of the plasma pressure (GPa) generated as function of the laser intensity (GW/cm^2) for the first and the second harmonic of Nd:YAG at 7 ns pulse duration and 21 ns (only for 1064 nm).

Table 2. Comparison between the first and the second harmonic, at 7 ns pulse duration.

λ (nm)	P_{max} (GPa)	I_{bk} (GW/cm^2)	α	Fitting law
1064	4.5	7	0.3	$P = 1.7 \sqrt{I}$
532 [17]	7	10	0.6	$P = 2.2 \sqrt{I}$

every addressed cases. Furthermore, the LSP process was historically developed at 1064 nm, and is still widely employed under this first harmonic of laser systems in industrial applications.

4. Understanding of the behavior of water confinement at high repetition rate

The water confinement behavior, especially its renewing time, has already been studied in previous work [26]. However, the acquisition frequency of the camera was limited to 20 000 FPS, and the laser frequency was simulated by using the same beam delayed up to 0.83 ms (equivalent laser frequency of 1.2 kHz). It was demonstrated that a water flow velocity of 10 m/s could allow the use of a repetition rate of 1 kHz for the laser.

In the present work, images are acquired up to 100 000 FPS, while the laser frequency reaching the target is tuned from 1 Hz to 200 Hz. Furthermore, not only the renewing time was measured: the ejected water was observed, and also the laser beam path where parasite breakdown plasmas were identified at such a high repetition rate. Finally, the sinking of treated samples was also measured as function of the laser frequency: this gives information about the true laser intensity that have reached the sample over thousands of shots.

4.1. Ejection of water

4.1.1. Geometry and velocities of ejection

Images obtained with the high-speed camera are plotted in Fig. 11 (acquisition frequency: 20 kHz) and Fig. 12 (acquisition frequency: 50 kHz). A background lighting was used to observe the ejected water.
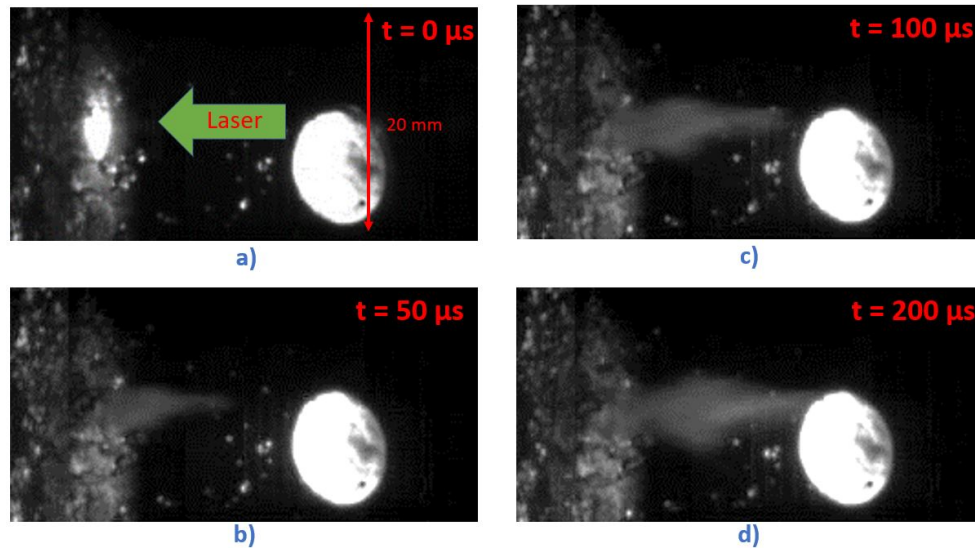
Fig. 11. High-speed camera observation (20k FPS) of the ejected water. Laser spot size: 0.72 mm, laser intensity: 1 GW/cm^2. a) t = 0 μs (laser pulse arrival) ; b) t = 50 μs ; c) t = 100 μs ; d) t = 200 μs.

Ejection velocities have been measured and reported to be between 20 to 800 m/s, and the angle of ejection from 0° to 45°. The drawing in Fig. 13 summarizes the different structures (and their associated velocities and angles) identified. Furthermore, these velocities are increasing with the laser intensity (it is doubled between 1 and 5 GW/cm^2). The same tendency is observed for the angles of ejection (the structure becomes more widely opened at higher laser intensities). These trends are expected as when the laser intensity increases, the total energy transferred to the plasma (and thus, the applied pressure that will eject the water) is also higher.

4.1.2.   Parasite breakdown plasmas

As illustrated in Fig. 14, some parasite plasmas have been observed along the laser beam path. We attributed these plasmas to the fact that after laser ablation and ejection of water, metal particles are also carried away by the water. As these particles are not transparent to the laser wavelength, it will initiate a lot of plasmas (by absorption of the laser energy) in the laser beam path. Furthermore, it may also be possible that the small drops of ejected water act as a short focal converging lens ; thus, the beam may be locally focused and high-intensities may be reached: this will initiate breakdowns in air or in water.

These plasmas are detrimental for the process as less energy will reach the surface, shot-by-shot.

To confirm this energy loss, the sinking of treated samples (LSP patch of 20 mm x 20 mm with an overlap ratio of 8000 % and a laser intensity of 4 GW/cm^2) has been measured as function of the used laser frequency, and is plotted in Fig. 15.

We can notice that the sinking is decreasing with the laser frequency, and with more sensibility when large spot sizes are used (as more water is ejected). Indeed, the sinking depth goes from 80 μm when samples were treated at 1 Hz to 48 μm at 200 Hz with a spot size of 2 mm, i.e a decrease of 40 %. This goes from 125 μm to 107 μm with a spot size of 0.72 mm, i.e a decrease of 15 %. However, the decrease is quite contained when going from 1 Hz to 25 Hz: 10 % with a 2 mm spot size and 4 % with a 0.72 mm spot size. Thus, it appears that this issue is relevant only at very high repetition rate (>50 Hz), which explains why no previous work has been reporting it since now.
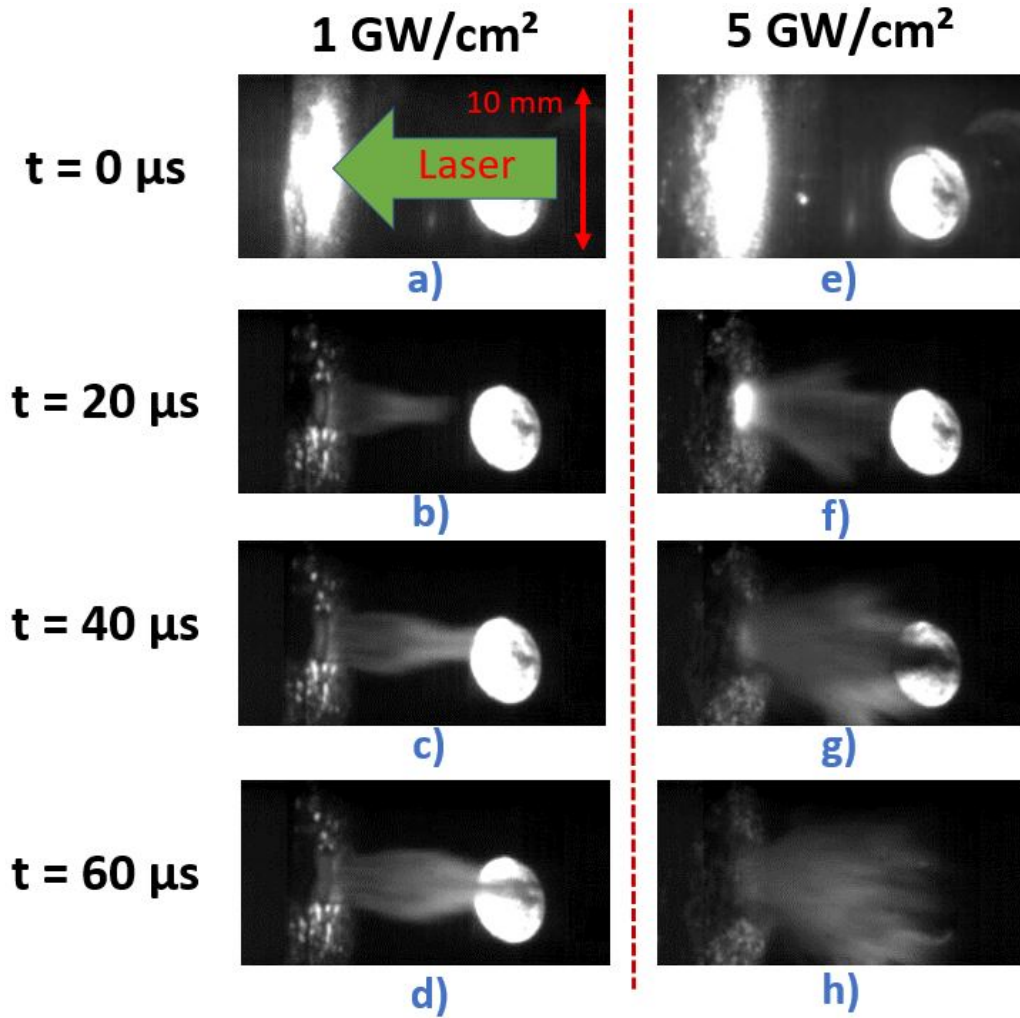
Fig. 12. High-speed camera observation (50k FPS) of the ejected water. Laser spot size: 0.72 mm, laser intensity: $I_1 = 1$ GW/cm^2 and $I_5 = 5$ GW/cm^2. a) t = 0 µs (laser pulse arrival), I_1 ; b) t = 20 µs, I_1 ; c) t = 40 µs, I_1 ; d) t = 60 µs, I_1 ; e) t = 0 µs (laser pulse arrival), I_5 ; f) t = 20 µs, I_5 ; g) t = 40 µs, I_5 ; h) t = 60 µs, I_5.

4.1.3. Required solution

As demonstrated, the ejected water is very fast (up to 800 m/s) and is carrying away metal particles that may either damage upstream optics or either harm the process with parasite plasmas (loss of energy). In order to thwart these two issues, we have implemented a air-blowing system (over-pressure up to 0.6 MPa), perpendicular to the beam path. This system (Fig. 16) has been demonstrated to be effective to solve these identified issues as shown by the sinking values plotted in Fig. 17. Indeed, the sinking values, when using our air blowing system, are almost the same (1 % to 9 % of relative difference) with no clear dependency with the used frequency.

Altogether, this kind of solution is necessary for the one who aims at performing LSP under such a high-repetition rate.
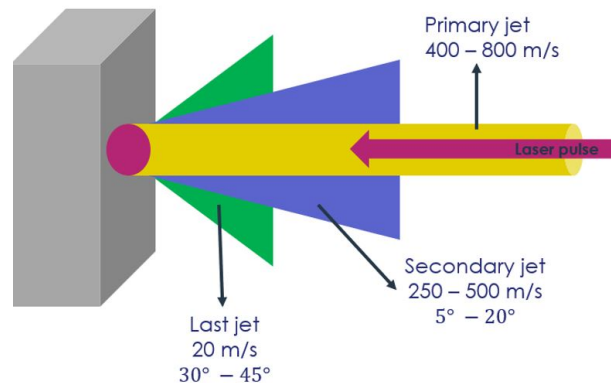
Fig. 13. Main structures identified, and their velocities (m/s) and angles (°), for the ejected water.
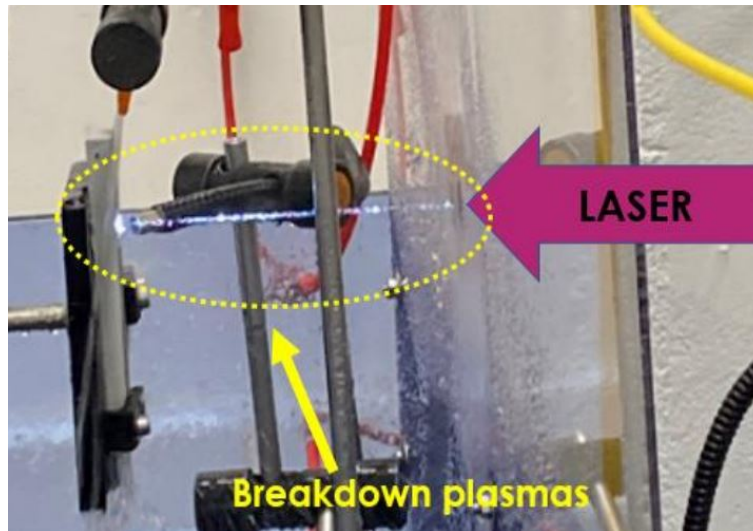

Fig. 14. Observation of parasite plasmas along the laser beam path at 200 Hz.

4.2. Renewing of water

In order to ensure a controlled and repeatable process, the water renewing frequency has been measured. The renewing time is defined as the time between the laser pulse arrival and the time for which the confinement is covering back again the whole laser spot surface, with no disturbance (Fig. 18).

The renewing frequency (Hz), as function of the water flow velocity (m/s), is plotted in Fig. 19. Two laser intensities have been investigated: 1 GW/cm^2 and 5 GW/cm^2 (0.72 mm spot size).

A renewing frequency of almost 200 Hz is reported when using a flow velocity of 1.2 m/s for both laser intensities. At higher flow rate, close to 6 m/s, the renewing frequency is approximately 1.8 kHz at 1 GW/cm^2 and 1.1 kHz at 5 GW/cm^2. These results demonstrate that with higher intensities, the water confinement is pushed away farther so that the renewing frequency is decreasing.

The same behaviour has been reported as function of the laser spot size, with a flow velocity of 6 m/s: 1.8 kHz at 0.72 mm, 1.6 kHz at 1.25 mm and 1.2 kHz at 2 mm.
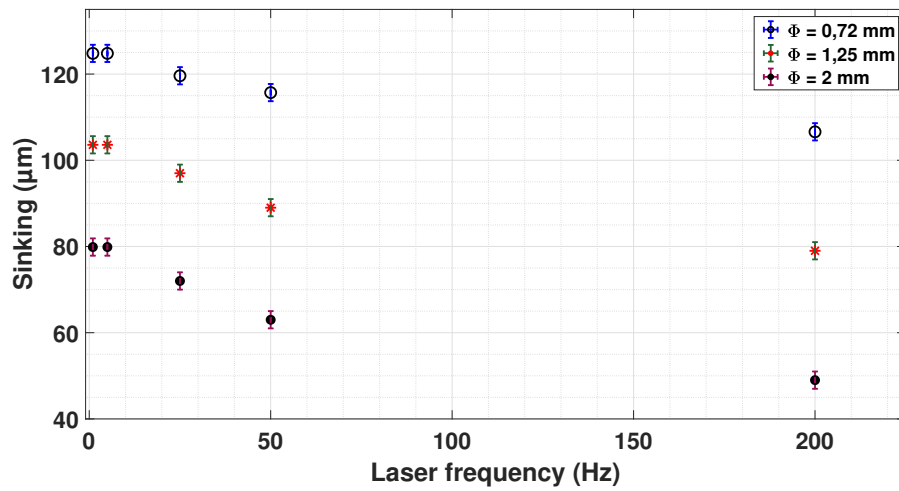
Fig. 15. Sinking (μm) of Al-samples after LSP treatment (8000%, 4 GW/cm^2) as function of the laser frequency for 3 spot sizes (0.72 mm, 1.25 mm and 2 mm).
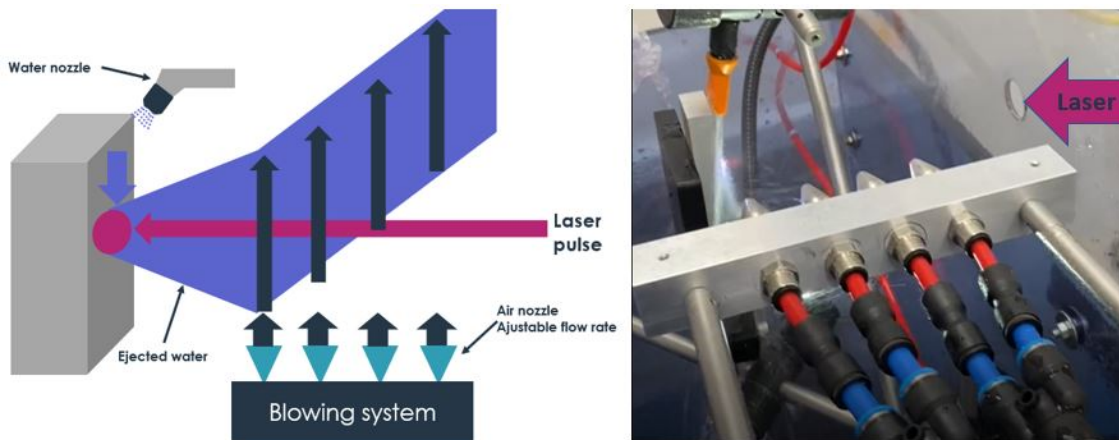

Fig. 16. Proposed air blowing system to thwart damages due to the ejected water.

Altogether, the renewing time will not be a critical phenomenon as very high frequencies may be used with relatively reachable water flow rates (3 m/s allows a frequency of 500 Hz for any cases). However, it has to be taken into account when developing a high frequency LSP solution.
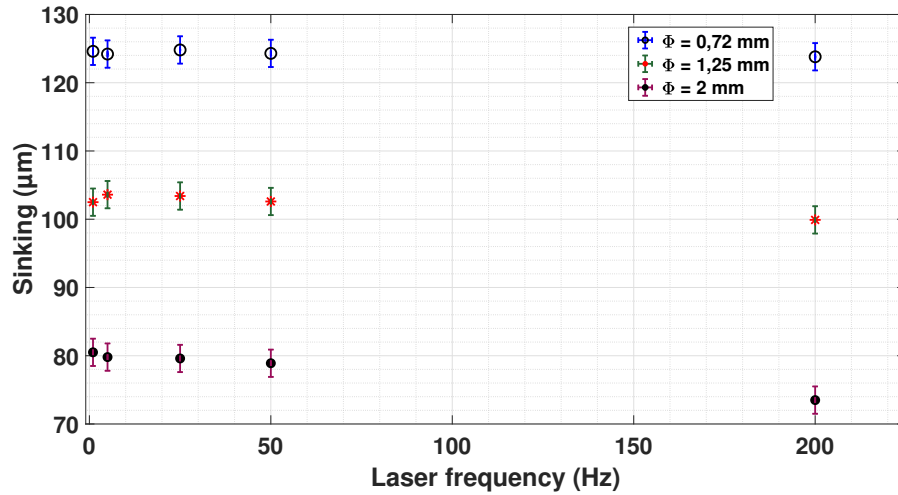
Fig. 17. Sinking (μm) of Al-samples after LSP treatment with our proposed air blowing system (over-pressure: 0.3 MPa). Treatments were performed with the same parameters as in Fig. 15.
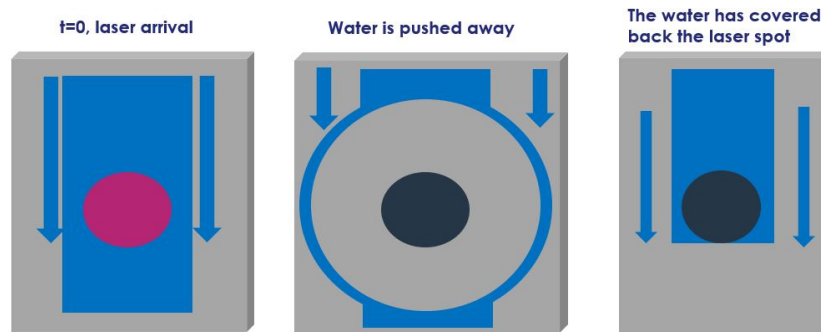

Fig. 18. Method used to measure the renewing time of the water confinement after a laser shot.
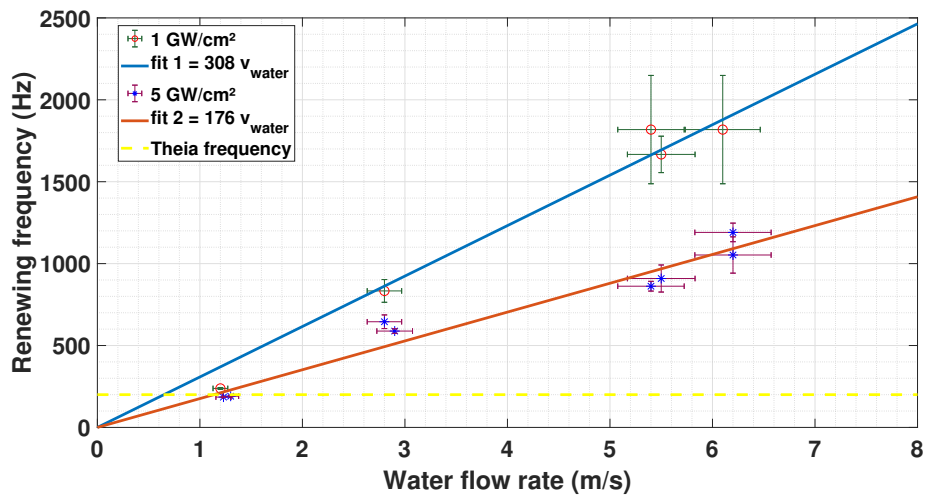

Fig. 19. Renewing frequency (Hz) as function of the water flow velocity (m/s) for 1 and 5 GW/cm^2, with 0.72 mm spot size. Linear fitting curves have been plotted.
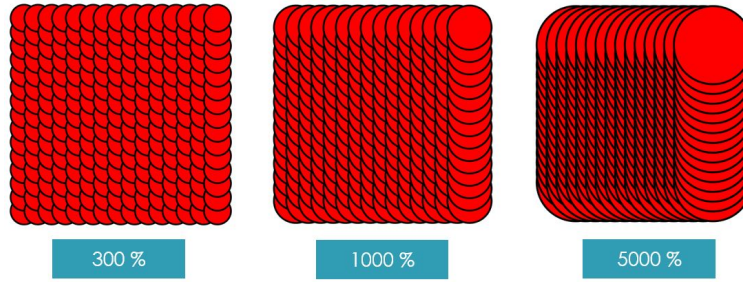
Fig. 20. Illustration of 3 different overlap ratios (300 %, 1000 % and 5000 %). Scales are different.

5. LSRDP Treatments of aluminum alloys

After having identified issues related to a high-repetition rate configuration (LSRDP), and after having implemented suitable solutions (as presented before in this paper), we have performed treatments on Al-2024 alloys used mainly in the aeronautical field. The main objective was to demonstrate that a high-repetition rate configuration, with small laser spot sizes, high overlap ratios and without any thermal coating, is operational.

Thus, consistently with our previous model on submillimeter plasmas (we expect the thermal loading of the plasma to be reduced with smaller laser spots so that the surface sample should not be under tensile residual stresses [14]), treatments were performed with 0.72 mm, 1.25 mm and 2 mm spot sizes, and results were compared. In the same way (we expect to reduce the tensile stress state when applying higher overlap ratios, as stated by Sano *et al.* [13]), overlap ratios from 300 % to 5000 % were used and investigated (Fig. 20).

The overlap ratio τ_r is defined by:

$$\tau_r \ (\%) = 100 \ \frac{\pi R^2}{D^2} \tag{5}$$

where R is the laser spot radius and D the laser displacement (center to center distance) between two successive shots. Knowing the laser frequency f and the robot velocity v_r (in front of the beam), we have: $fD = v_r$.

For all-presented cases, the laser intensity was 4 GW/cm^2, the gaussian laser pulse duration (FWHM) 6.9 ns and the wavelength 1064 nm. Residual stress fields were measured through $\sin^2(\Psi)$ XRD method.

The obtained results are plotted in Fig. 21 (effect of the spot size) and in Fig. 22 (effect of the overlap ratio). The reference sample stress state, which corresponds to the same sample but without LSP treatment, is also plotted.

For any cases with LSRDP treatments, the in-depth profile is encouraging as it shows typical values of compressive state, as obtained in the literature. Thus, this demonstrates the capability of LSRDP to be applied and further investigated.

However, regarding the surface state, each configuration does not necessarily bring improvements compared to the reference sample. Indeed, we obtain respectively 0 MPa, -30 MPa and -198 MPa for 2 mm, 1.25 mm and 0.72 mm spot sizes (Fig. 21), while this was -134 MPa for the reference sample. Nevertheless, these results are in a good agreement with our previous model as they demonstrate that the surface state becomes more compressive when using smaller laser spot sizes.

Regarding the impact of the overlap ratio, the surface state is respectively -12 MPa, -109 MPa and -198 MPa for 300 %, 1000 % and 5000 %. Consistently with the literature, this confirms that
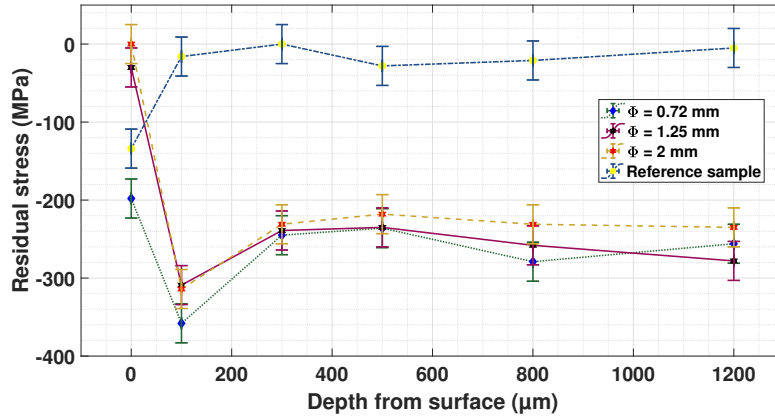
Fig. 21. In-depth (μm) residual stress (MPa) profiles measured on Al-2024 for 3 spot sizes: 0.72 mm, 1.25 mm and 2 mm. The overlap ratio is 5000 %.
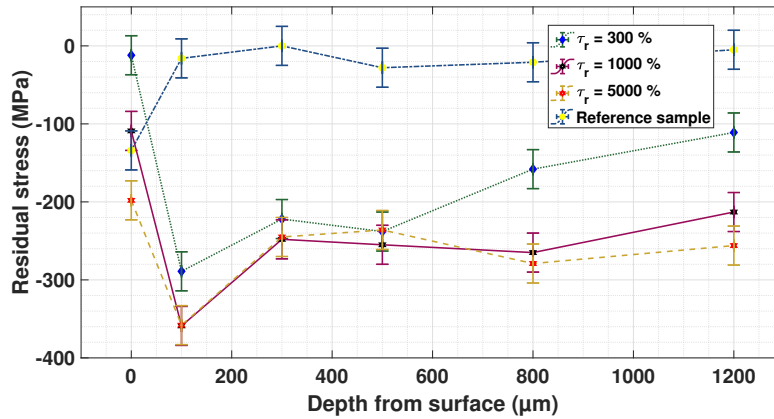

Fig. 22. In-depth (μm) residual stress (MPa) profiles measured on Al-2024 for 3 overlap ratios: 300 %, 1000 % and 5000 %. The laser spot size is 0.72 mm.

higher overlap ratios may help to fight tensile residual stresses on the surface when applying LSP without coating.

Therefore, these results demonstrate the feasibility of our presented LSRDP configuration. Moreover, even though small laser spot sizes are recommended, as well as high overlap ratios to avoid detrimental tensile residual stresses, our configuration remains competitive regarding the time required to treat a given surface, thanks to the THEIA laser high frequency.

Deep compressive residual stress profiles are obtained (up to more than 1 mm), and they should be investigated with fatigue tests in the near future.

6. Conclusion

In this paper, we have presented a new DPSS Nd:YAG laser system delivering 1 J of energy, with ns-range pulses, and working at a high frequency of 200 Hz. Thanks to this laser, we investigated a new configuration for the laser shock peening process: with small laser spots, with high overlap ratios, without thermal coating and at high-repetition rate.

At such rates, difficulties were highlighted regarding the behaviour of the water used as confinement. A air blowing system has been shown to be required to protect upstream optics and to avoid detrimental parasite plasmas, that limit the laser energy involved in the process. Moreover, the possible frequency at which one may use this configuration has been obtained as function of the water flow velocity. At 200 Hz, a minimum value of 2 m/s is recommended. Furthermore, our results and previous works also underline that the green visible wavelength (532 nm) may be better (higher absorption efficiency and higher breakdown thresholds with short ns pulses). In addition, better SHG efficiency is obtained with shorter pulses.

We have demonstrated the effectiveness of this fast configuration to reinforce aluminium alloys by LSP. However, further developments should now concentrate on the optimization of the resulting improvements in fatigue life, with regards to the used laser parameters. Using this configuration, new applications may be addressed especially as this laser system may be injected into an optical fiber, then bringing maneuverability and security to the process.

Future improvements should appear, such as laser frequencies up to 500 Hz, and thus this will help the deployment of the LSRDP configuration.

Disclosures. The authors declare no conflicts of interest.

Data availability. Data underlying the results presented in this paper are are available from the corresponding author upon reasonable request.

References

1. M. Sagnard, R. Ecault, F. Touchard, M. Boustie, and L. Berthe, "Development of the symmetrical laser shock test for weak bond inspection," Optics and Laser Technology **111**, 644–652 (2018).
2. R. Ecault, F. Touchard, L. Berthe, and M. Boustie, "Laser shock adhesion test numerical optimization for composite bonding assessment," Composite Structures **247**, 112441 (2020).
3. P. Peyre, R. Fabbro, P. Merrien, and H. P. Lieurade, "Laser shock processing of aluminium alloys. application to high cycle fatigue behaviour," Materials Science and Engineering: A **210**(1-2), 102–113 (1996).
4. Y. Sano, N. Mukai, M. Yoda, T. Uehara, I. Chida, and M. Obata, "Development and applications of laser peening without coating as a surface enhancement technology," Proc. of SPIE 6343, 1–12 (2006).
5. D. Furfari, "Laser shock peening to repair, design and manufacture current and future aircraft structures by residual stress engineering," Adv. Mater. Res. **891-892**, 992–1000 (2014).
6. N. Kashaev, V. Ventzke, M. Horstmann, S. Chupakhin, S. Riekehr, R. Falck, E. Maawad, P. Staron, N. Schell, and N. Huber, "Effects of laser shock peening on the microstructure and fatigue crack propagation behaviour of thin AA2024 specimens," Int. J. Fatigue **98**, 223–233 (2017).
7. N. C. Anderholm, "Laser-generated stress waves," Appl. Phys. Lett. **16**(3), 113–115 (1970).
8. R. Fabbro, J. Fournier, P. Ballard, D. Devaux, and J. Virmont, "Physical study of laser?produced plasma in confined geometry," J. Appl. Phys. **68**(2), 775–784 (1990).
9. T. Sakka, K. Takatani, Y. Ogata, and M. Mabuchi, "Laser ablation at the solid-liquid interface: transient absorption of continuous spectral emission by ablated aluminium atoms," J. Phys. D: Appl. Phys. **35**(1), 65–73 (2002).
10. P. Cary, History of the Shot Peening, *Int. Conf. Shot Peening, ICPS-1, Paris* (1981).
11. Y. Sano, N. Mukai, K. Okazaki, and M. Obata, "Residual stress improvement in metal surface by underwater laser irradiation," Nuclear Instruments and Methods in Physics Research **121**(1-4), 432–436 (1997).
12. Y. Sano, "Quarter century development of laser peening without coating," Metals **10**(1), 152 (2020).
13. Y. Sano, K. Akita, and T. Sano, "A Mechanism for Inducing Compressive Residual Stresses on a Surface by Laser Peening without Coating," Metals **10**(6), 816 (2020).
14. A. Rondepierre, S. Unaldi, Y. Rouchausse, L. Videau, R. Fabbro, O. Casagrande, C. Simon-Boisson, H. Besaucèle, O. Castelnau, and L. Berthe, "Beam size dependency of a laser-induced plasma in confined regime: Shortening of the plasma release. Influence on pressure and thermal loading," Optics and Laser Technology **135**, 106689 (2021).

15. A. Clauer, "Laser shock peening, the path to production," Metals **9**(6), 626 (2019).

16. J. Körner, S. Zulic, J. Reiter, M. Lenski, J. Hein, R. Bödefeld, D. Rostohar, T. Mocek, and M. Kaluza, "Compact, diode-pumped, unstable cavity yb:yag and its application in laser shock peening," Opt. Express **29**(10), 15724–15732 (2021).

17. A. Rondepierre, Y. Rouchausse, L. Videau, O. Casagrande, O. Castelnau, and L. Berthe, "Laser interaction in a water tank configuration: Higher confinement breakdown threshold and greater generated pressures for laser shock peening," Journal of Laser Application **33**(4), 042022 (2021).

18. L. Barker and R. Hollenbach, "Laser interferometer for measuring high velocities of any reflecting surface," J. Appl. Phys. **43**(11), 4669–4675 (1972).

19. U. Welzel, J. Ligot, P. Lamparter, A. Vermeulen, and E. Mittemeijer, "Stress analysis of polycristalline thin films and surface regions by X-ray diffraction," J. Appl. Crystallogr. **38**(1), 1–29 (2005).

20. P. Peyre, L. Berthe, V. Vignal, I. Popa, and T. Baudin, "Analysis of laser shock waves and resulting surface deformations in an al–cu–li aluminum alloy," J. Phys. D: Appl. Phys. **45**(33), 335304 (2012).

21. A. Sollier, Etude des plasmas générés par interaction laser-matière en régime confiné : application au traitement des matériaux par choc laser, Ph.D. thesis, Université de Versailles St-Quentin (2002). Thèse de doctorat dirigée par Fabbro, Rémy Physique Versailles-St Quentin en Yvelines 2002.

22. A. Sollier, L. Berthe, and R. Fabbro, "Numerical modeling of the transmission of breakdown plasma generated in water during laser shock processing," The European Physical Journal - Applied Physics **16**(2), 131–139 (2001).

23. F. Docchio, C. Sacchi, and J. Marshall, "Experimental investigation of optical breakdown thresholds in ocular media under single pulse irradiation with different pulse durations," Laser in Ophtalmology **1**, 83–93 (1986).

24. C. Max, "Theory of the coronal plasma in laser-fusion targets," Physics of laser fusion **I** (1981).

25. C. Garban-Labaune, E. Fabre, C. Max, F. Amiranoff, R. Fabbro, J. Virmont, and W. Mead, "Experimental results and theoretical analysis of the effect of wavelength absorption and hot-electron generation in laser-plasma interaction," The Physics of Fluids **28**(8), 2580–2590 (1985).

26. L. Berthe, D. Courapied, S. El Karnighi, P. Peyre, C. Gorny, and Y. Rouchausse, "Study of laser interaction in water flow confinement at high repetition rate," J. Laser Appl. **29**(4), 042006 (2017).